Proceedings of IMECE2006
2006 ASME International Mechanical Engineering Congress and Exposition
November 5-10, 2006, Chicago, Illinois, USA

IMECE2006-16305

MOLECULAR DYNAMICS STUDY OF SHORT-PULSE LASER MELTING, RECRYSTALLIZATION, SPALLATION, AND ABLATION OF METAL TARGETS

Leonid V. Zhigilei
Department of Material Science and Engineering
University of Virginia
Charlottesville, VA 22904
lz2n@virginia.edu

Zhibin Lin
Department of Material Science and Engineering
University of Virginia
Charlottesville, VA 22904
zl5c@virginia.edu

http://www.faculty.virginia.edu/CompMat/

Dmitriy S. Ivanov
National Centre for Laser Applications
National University of Ireland
Galway, Ireland
dmitriy@nuigalway.ie

ABSTRACT

A hybrid computational model combining classical molecular dynamics method for simulation of fast non-equilibrium phase transformations with a continuum description of the laser excitation and subsequent relaxation of the conduction band electrons is developed. The model is applied for a systematic computational investigation of the mechanisms of short pulse laser interaction with bulk metal targets. The material response to laser irradiation is investigated in three regimes corresponding to the melting and resolidification of the surface region of the target, photomechanical spallation of a single or multiple layers/droplets, and ablation driven by the thermodynamic driving forces. The conditions leading to the transitions between the different regimes and the atomic-level characteristics of the involved processes are established.

1. INTRODUCTION

Short-pulse laser irradiation can induce a range of non-equilibrium processes in a target material, from strong overheating and melting, to the ultrafast deformation and photomechanical damage, to an explosive disintegration and massive material removal (ablation). Analysis of the laser-induced processes leads to a range of important fundamental questions, such as the limit of superheating and the microscopic mechanisms of homogeneous and heterogeneous melting, the nature of the fracture/spallation at ultra-high deformation rates and elevated temperatures, as well as the mechanisms of explosive boiling and disintegration of material in laser ablation.

Atomic-level computer modeling has the ability to provide detailed information on the complex processes induced by the fast laser energy deposition and can assist in the advancement of laser-driven applications, e.g. [1-7]. Recent development of a hybrid computational model that combines classical molecular dynamics (MD) method for simulation of fast non-equilibrium phase transformations in the target material with a continuum description of the laser excitation and subsequent relaxation of the conduction band electrons based on the two-temperature model (TTM), has opened new opportunities for

detailed investigation of a variety of phenomena in laser interactions with metal targets. First applications of the TTM-MD model have already provided insights into the microscopic mechanisms of laser melting and disintegration of Ni and Au films [8-11], photomechanical spallation of Cu and Ni targets [12,13]. The hybrid TTM-MD model was also used in a recent study of shock-induced heating and melting of a grain boundary region in an Al crystal [14] and in the analysis of the kinetics and channels of laser energy redistribution in a Ni target irradiated by a short laser pulse [15].

In this paper we present a systematic analysis of short pulse laser interactions with bulk Ni targets. The range of laser fluences used in the simulations is chosen to cover different regimes of the material response to laser heating, from transient melting and resolidification, to photomechanical spallation, and to the ablation driven by the thermodynamic driving forces. The conditions leading to the transitions between different regimes in material response to laser irradiation are established A brief description of the combined TTM-MD model as well as the parameters of the model used in the simulations presented in this paper are given below, in Section 2. The results of the simulations of laser melting, spallation and ablation of Ni targets are presented in Section 3 and summarized in Section 4.

2. COMBINED TTM - MD MODEL

The classical MD method does not include an explicit representation of electrons and, as a result, cannot be used to model the laser energy absorption by the conduction band electrons and the energy transfer from the excited electrons to the lattice. Moreover, since the electronic contribution to the thermal conductivity of a metal is dominant, the conventional MD method, where only the lattice contribution is present, significantly underestimates the total thermal conductivity. This leads to unphysical confinement of the deposited laser energy in the surface region of the irradiated target and does not allow for direct comparison between the calculated and experimental data. A computational model aiming at overcoming these limitations and combining the advantages of TTM, commonly used in continuum-level modeling of short pulse laser interactions with metals, and MD is briefly described below. A complete description of the combined TTM-MD model has been reported elsewhere [8].

In the combined model the MD method completely substitutes the TTM equation for the lattice temperature. The diffusion equation for electron temperature, T_e, is solved by a finite difference method simultaneously with MD integration of the equations of motion of atoms,

$$\text{TTM:}\quad C_e(T_e)\frac{\partial T_e}{\partial t} = \nabla\left(K_e(T_e, T_l)\nabla T_e\right) - G(T_e - T_l) + S(z,t)$$

$$\text{MD:}\quad m_i\frac{d^2\vec{r}_i}{dt^2} = \vec{F}_i + \xi m_i \vec{v}_i^{\,T}, \qquad T_l^{cell} = \sum_{i=1}^{N^{cell}} m_i\left(\vec{v}_i^{\,T}\right)^2 \Big/ \left(3k_B N^{cell}\right)$$

where C_e is the electron heat capacity, K_e is the electron thermal conductivity, G is the electron-phonon coupling factor, and the source term S(z,t) is used to describe the local laser energy deposition per unit area and unit time during the laser pulse duration. In the MD part of the model, m_i and r_i are mass and position of an atom i, F_i is the force acting on atom i due to the interatomic interactions. An additional term, $\xi m_i \vec{v}_i^{\,T}$, is added to the ordinary MD equations of motion to account for the electron-phonon coupling. The cells in the finite difference discretization are related to the corresponding volumes of the MD system and the local lattice temperature, T_l^{cell}, is calculated for each cell from the average kinetic energy of the thermal motion of atoms. Thermal velocity of an atom is defined as $\vec{v}_i^{\,T} = \vec{v}_i - \vec{v}^{\,c}$, where $\vec{v}_i$ is the actual velocity of an atom i, and $\vec{v}^{\,c}$ is the velocity of the center of mass of a cell to which atom i belongs. The expansion, density variations, and, at higher fluences, disintegration of the irradiated target predicted in the MD part of the model are accounted for in the continuum part of the model [8].

The hybrid approach, briefly described above, combines the advantages of the two-temperature model and the MD method. The two-temperature model provides an adequate description of the laser energy absorption into the electronic system, energy exchange between the electrons and phonons, and fast electron heat conduction in metals, whereas the MD method is appropriate for simulation of non-equilibrium processes of lattice superheating, melting, and ablation.

In this work we apply the TTM-MD model to study the laser melting, spallation and ablation of bulk Ni targets. The MD method is used only in the top surface region of the target, whereas the diffusion equation for electron temperature is solved in a much wider 1 μm region, providing an adequate representation of the electronic heat conduction into the bulk of the target. A strong electron–phonon coupling and a relatively small thermal diffusivity (as compared with other metals) in Ni leads to a rapid transfer of the absorbed energy from the excited electrons to the lattice and confines the initial laser energy deposition in a shallow surface region of the target. The energy confinement allows for a realistic simulation of laser interaction with a bulk target with a depth of the MD part of the combined model as small as 100 nm for low fluences, below the threshold for laser spallation, and 200 nm at higher fluences, in the spallation and ablation regimes. The lateral dimensions of the MD computational cell are 3.53 × 3.53 nm, with 113600 and 227200 atoms in the 100 and 200 nm cells, respectively. Periodic boundary conditions are applied in the lateral directions, parallel to (100) free surface of the initial FCC crystals. Before applying laser irradiation, the initial systems are equilibrated at 300 K.

In order to avoid reflection of the pressure waves propagating from the irradiated surface, the dynamic pressure-transmitting boundary condition [16] is applied at the bottom of the MD region. The boundary condition simulates the propagation of the laser-induced pressure wave from the surface region of the target represented by the MD method to the continuum part of the model. The energy carried away by

the pressure wave is monitored, allowing for control over the total energy conservation in the combined model. In the continuum part of the model, beyond the MD region, the energy exchange between the electrons and the lattice is described by the conventional TTM. The temperature dependence of the lattice heat capacity, obtained for the model material, is approximated by a polynomial function and is used in the TTM equation for the lattice temperature.

The thermal and elastic properties of the lattice, such as the lattice heat capacity, elastic moduli, coefficient of thermal expansion, melting temperature, volume and entropy of melting and vaporization, etc., are all defined by the interatomic interaction, described in this work by the embedded-atom method (EAM) in the form suggested in Ref. [17]. Some of the parameters of the model EAM Ni material are reported in [8,18]. The parameters used in the TTM equation for the electron temperature are listed below. The electronic heat capacity is $C_e = \gamma T_e$ with $\gamma = 1065$ $Jm^{-3}K^{-2}$, the thermal conductivity is $K_e = K_0 T_e/T_l$ with $K_0 = 91$ $Wm^{-1}K^{-1}$, the electron–phonon coupling factor is $G = 3.6\times10^{17}$ $Wm^{-3}K^{-1}$, and the optical absorption depth is Lp = 13.5 nm. A justification of the choice of the approximation used to describe the dependence of the electron thermal conductivity K_e on the electron and lattice temperatures is given in Ref. [8]. Laser pulse duration of 1 ps is used in the simulations and the absorbed laser fluence rather then the incident fluence is used in the discussion of the simulation results.

3. RESULTS OF THE SIMULATIONS

The results of the simulations of laser interaction with a bulk Ni target are described in this section for laser fluences ranging from the one close to the threshold for the onset of laser melting and up to the fluence leading to the explosive decomposition of the surface region overheated up to the critical temperature of the model material.

3.1 Laser melting and resolidification

The absorbed fluence threshold for laser melting of bulk EAM Ni target has been determined in Ref. [10] to be 36 mJ/cm^2. The threshold is arbitrary defined as a fluence at which the maximum number of atoms in the liquid phase during the simulation corresponds to that in a 2 nm layer in the initial crystal before the irradiation. The liquid phase is identified based on the local order parameter defined in Ref. [8].

A simulation performed at a fluence of 43 mJ/cm^2, about 20% above the melting threshold, is illustrated by the temperature and pressure contour plots shown in Figure 1. Fast energy transfer from the hot electrons excited by the laser pulse to the lattice leads to the temperature increase in the surface region of the target, Figure 1a. Strong electron-phonon coupling in Ni results in the initial confinement of a large portion of the deposited laser energy within the top 50 nm region of the target. The lattice heating leads to a fast melting of ~15 nm surface layer of the target at ~12-20 ps after the laser pulse. The melting results in a transient decrease of the lattice temperature near the melting front due to the transfer of a part of the thermal energy to the latent heat of melting. The evolution of the temperature at later time is mainly defined by the fast electronic heat conduction to the bulk of the target. The temperature field is continuous at the boundary separating the MD and continuum parts of the model, reflecting a seamless transition between the two parts of the model. The melting is followed by epitaxial recrystallization that is completed by the time of 250 ps after the laser pulse.

The fast temperature increase, occurring under conditions of the inertial stress confinement [13], leads to the compressive pressure buildup which, in turn, relaxes by driving a compressive pressure wave deeper into the bulk of the target and inducing an unloading tensile wave that follows the compressive component, Figure 1b. Both the compressive and tensile components of the pressure wave propagate without any noticeable reflection from the boundary separating the MD and continuum parts of the model, indicating that the pressure-transmitting boundary condition is working correctly.

The condition for the stress confinement, required for the generation of a strong thermoelastic pressure wave in the metal target can be expressed as $\max\{\tau_p, \tau_{e\text{-}ph}\} \le \tau_s \sim L_c/C_s$, where τ_p is the laser pulse duration, $\tau_{e\text{-}ph}$ is the characteristic time of the energy transfer from the excited hot electrons to the lattice, and τ_s is the time required for the relaxation of the laser-induced stresses, defined by the diffusive/ballistic penetration depth of the excited electrons before the electron–phonon equilibration L_C and speed of sound in the target material C_S. For Ni, $\tau_{e\text{-}ph} \approx 5$ ps [8], $L_C \approx 50$ nm [10], and the condition for the stress confinement is satisfied for 1 ps laser pulse irradiation.

An abrupt change in the pressure values upon crossing the crystal-liquid interface in Figure 1b is related to the confinement of the heated crystalline material in the lateral directions [13]. For a typical laser spot diameter of ~100 μm, the fast relaxation of the laser-induced pressure can only proceed in the direction normal to the surface. These conditions of lateral confinement are correctly reproduced by the periodic boundary conditions used in the directions parallel to the surface. In the melted part of the target the stresses remain isotropic during the uniaxial expansion of the surface region and the pressure is defined only by the volume and temperature. The uniaxial expansion of the crystalline part of the target, however, results in anisotropic lattice deformations and corresponding anisotropic stresses. The anisotropic stresses in a crystal cannot relax by uniaxial expansion and the residual compressive stresses remain in the crystalline part of the target long after the relaxation of the transient thermoelastic stresses in the melted part. The residual uniaxial lattice expansion can be related to experimental measurements of

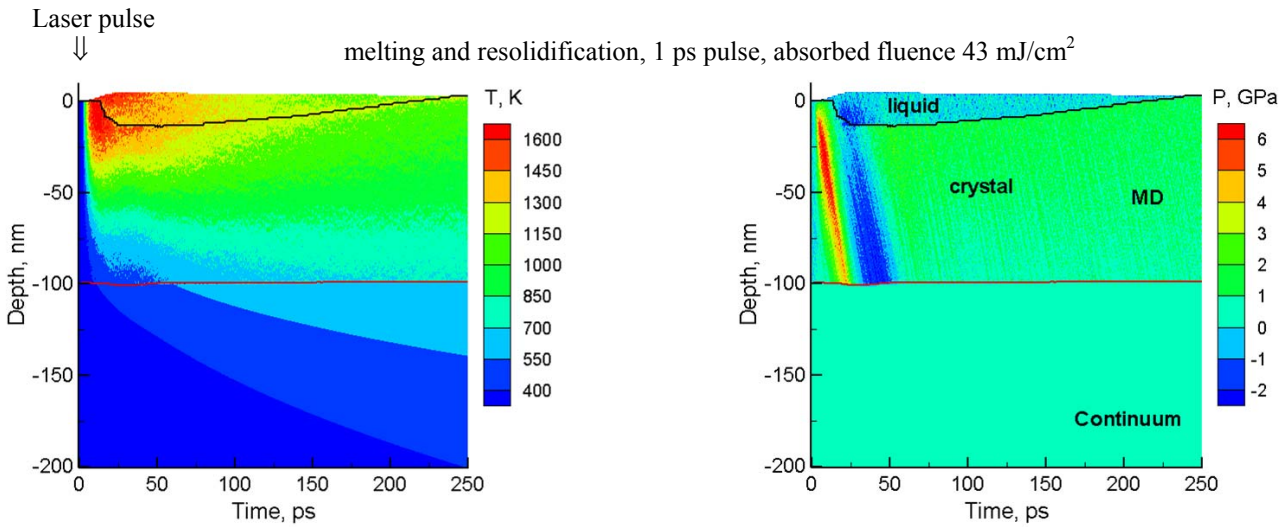

Figure 1. Temperature (a) and pressure (b) contour plots in a simulation of melting and resolidification of a bulk Ni target irradiated with a 1 ps laser pulse at an absorbed fluence of 43 mJ/cm^2, close to the threshold for the surface melting. Laser pulse is directed along the Y-axes, from the top of the contour plots. Black line separates the melted region from the crystalline bulk of the target. Red line separates the MD and continuum parts of the combined TTM-MD model.

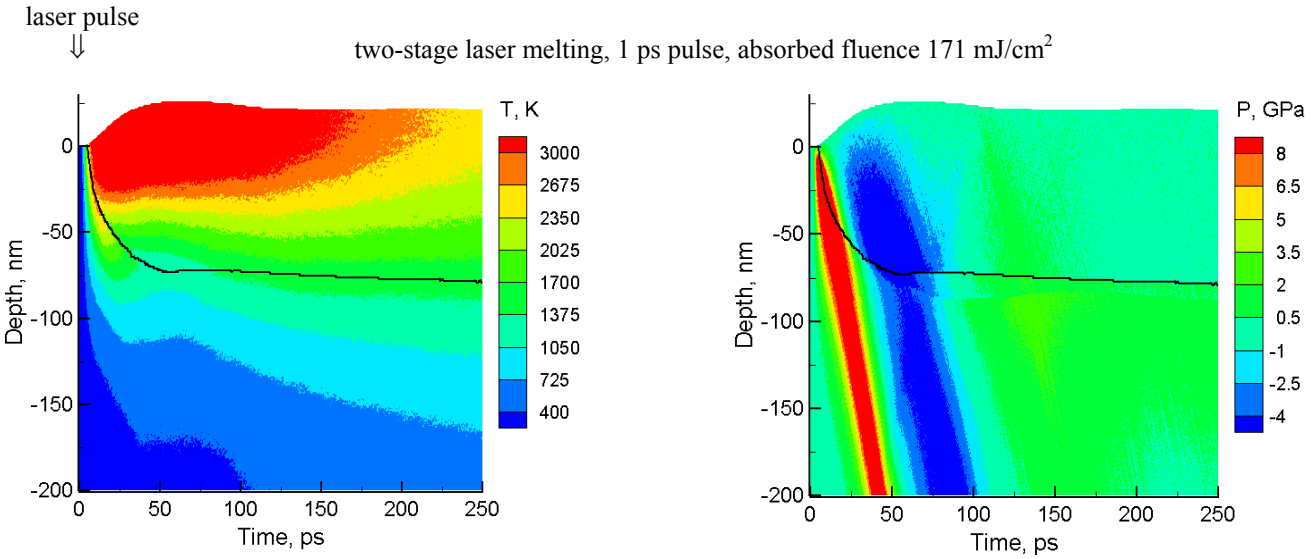

Figure 2. Temperature (a) and pressure (b) contour plots in a simulation of laser melting of a bulk Ni target irradiated with a 1 ps laser pulse at an absorbed fluence of 171 mJ/cm^2, just below the threshold for laser spallation. Laser pulse is directed along the Y-axes, from the top of the contour plots. Black line separates the melted region from the crystalline bulk of the target.

lattice deformation performed with time-resolved X-ray diffraction for Pt(111) crystals irradiated by a nanosecond laser pulse [19]. The measured evolution of the lattice strain is found to be strongly affected by the conditions of the lateral confinement leading to the one-dimensional lattice expansion.

An increase of the laser fluence further above the threshold for laser melting leads to the increase of both the maximum melting depth and the time of recrystallization. A simulation performed at a fluence of 171 mJ/cm^2, 4.75 times the melting threshold fluence is illustrated in Figure 2. Two stages of laser melting can be clearly identified in this simulation – fast melting of more than 50 nm of the target within the first 30 ps after the laser pulse and a much slower melting of additional 15 nm within ~500 ps. A detailed atomic-level analysis of the melting process demonstrates that massive homogeneous nucleation of the liquid phase inside the overheated crystal is responsible for the fast component of the melting process (see Figure 7a), whereas the propagation of a well-defined

liquid-crystal interface deeper into the target is responsible for the slower component of the melting process. The picture of the two-stage melting obtained in the simulations can be related to experimental observations reported in Ref. [20], where time-resolved reflectivity measurements reveal a fast (5-10 ps) and slow (100s ps) melting stages for GaAs irradiated by a femtosecond pulse in the "thermal melting" regime.

Comparison of the temperature and pressure contour plots, Figures 2a and 2b, suggests that an apparent "shoulder" in the temperature distribution at ~20-80 ps correlates with the passage of the laser-induced pressure wave. Propagation of the tensile wave leads to a pronounced transient cooling of the material. Similar temperature–pressure correlations have been also observed in simulations of laser interaction with metal films [8,9]. Considering a fast adiabatic/isentropic compression or expansion of a material, the temperature variation with pressure can be estimated from classical thermodynamics,

$$\left(\frac{\partial T}{\partial P}\right)_S = \frac{VT\alpha}{C_P} > 0,$$

where the heat capacity C_P, volume V, and the volume coefficient of thermal expansion α are all positive for Ni. Thus, the compressive part of the laser-induced bimodal pressure wave contributes to the heating of the target material, whereas the expansion during the passage of the unloading component results in a transient cooling.

3.2 Laser spallation

The increase of the laser fluence above 171 mJ/cm^2 is found to lead to the spallation – a separation of a layer of liquid material from the bulk of the target. The threshold fluence for the separation of a layer from a bulk Ni target is found to be between 171 mJ/cm^2 (Figure 2 – no layer ejection) and 193.5 mJ/cm^2 (Figure 3 – ejection of a ~25 nm-thick liquid layer). The separation and ejection of the liquid layer takes place by the nucleation, growth and coalescence of multiple voids in a subsurface region of the target. The appearance of the voids coincides with the arrival of the unloading tensile wave that propagates from the surface and increases its strength with depth. The mechanical stability of the region subjected to the void nucleation is strongly affected by the laser heating and the depth of the spallation region in bulk targets is much closer to the surface as compared with the depth where the maximum tensile stresses are generated, Figure 3b.

An atomic-level picture of a void generated in the process of laser spallation is shown in Figure 7b. Only several gas phase atoms are observed inside the growing void, indicating that the process of void nucleation and growth is driven by the relaxation of the laser-induced thermoelastic stresses and is not related to boiling. The results of earlier molecular dynamics simulations of laser irradiation of bulk molecular targets [2,21,22] and metal films [8,18] suggest that photomechanical spallation is a general process that can occur in a wide class of materials and different types of targets. The mechanisms of spallation are found to be similar in molecular and metal targets and are described in details in Ref. [13].

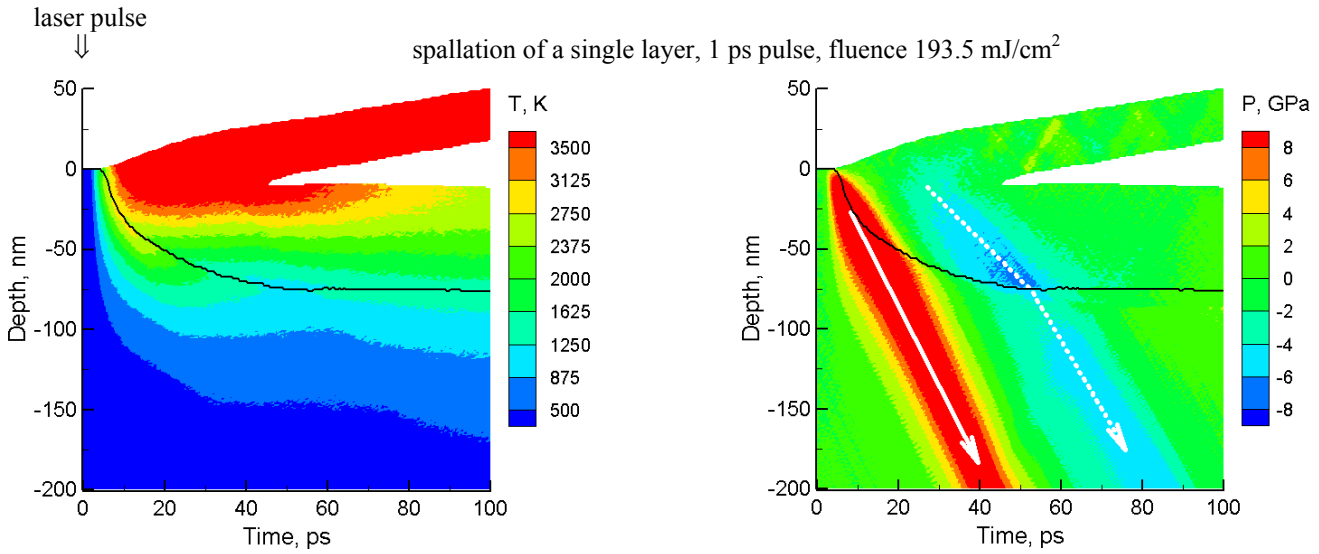

Figure 3. Temperature (a) and pressure (b) contour plots in a simulation of laser spallation of a bulk Ni target irradiated with a 1 ps laser pulse at an absorbed fluence of 193.5 mJ/cm^2, just above the threshold for laser spallation. Laser pulse is directed along the Y-axes, from the top of the contour plots. Black line separates the melted region from the crystalline bulk of the target. Areas where the density of the material is less than 10% of the initial density before the irradiation are not shown in the plots.

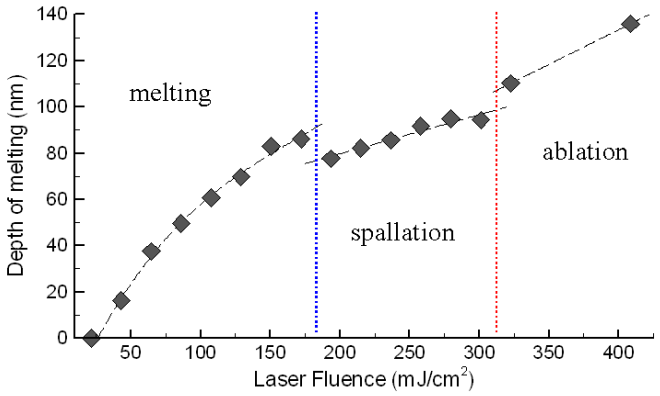

Figure 4. Maximum melting depth as a function of laser fluence in simulations of 1 ps laser interaction with bulk Ni targets.

In all the simulations performed so far spallation is always preceded by melting, no spallation of solid target has been observed. Interestingly, the maximum melting depth that has been steadily growing with fluence up to the ablation threshold experiences an abrupt drop at the spallation threshold, Figure 4. This observation can be explained by the fact that the spallation interrupts the electronic heat conduction from the hot surface region to the bulk of the target, Figure 3a. As a result, the amount of heat transferred to the liquid-crystal interface from the surface region decreases, the second (slow, heterogeneous) stage of the melting process discussed in Section 3.1 shortens, and the maximum melting depth drops.

Further increase of the laser fluence above the spallation threshold result in the spallation of multiple layers/clusters from the target, as illustrated by the results obtained for laser fluence of 279.5 mJ/cm^2, Figure 5. At this laser fluence the surface layer is strongly overheated and readily disintegrates at moderate tensile stresses. Note that the temperature of the surface region of the target still remains significantly below the critical temperature and thermodynamic driving forces alone are not sufficient to cause a collective material ejection. At the maximum surface temperature realized in this simulation the material ejection would be limited to surface evaporation if not for the assistance of the unloading wave. Therefore, despite the relatively high laser fluence and surface temperature, we still classify the process leading to the ejection of liquid droplets in this simulation as spallation.

3.3 Laser ablation driven by thermodynamic driving forces

At laser fluence above ~320 mJ/cm^2, the surface region of the irradiated target reaches the limit of it's thermodynamic stability and the main process responsible for the material ejection changes to the explosive decomposition of the overheated material into a mixture of vapor and liquid droplets. An example illustrating this ablation mechanism is shown in Figure 6. A surface region that exceeds or approaches the critical temperature becomes unstable and disintegrates in an explosive manner. A snapshot from the ablation plume consisting of the gas-phase atoms and small clusters is shown in Figure 7c.

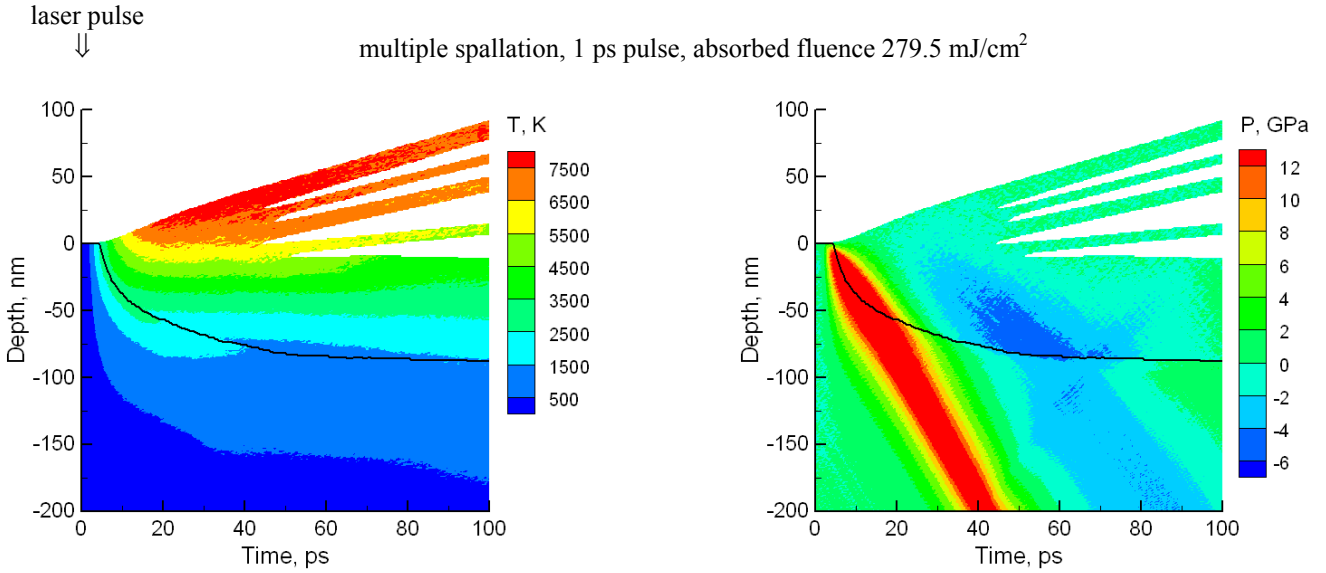

Figure 5. Temperature (a) and pressure (b) contour plots in a simulation of multiple spallation of a bulk Ni target irradiated with a 1 ps laser pulse at an absorbed fluence of 279.5 mJ/cm^2, just above the threshold for laser spallation. Laser pulse is directed along the Y-axes, from the top of the contour plots. Black line separates the melted region from the crystalline bulk of the target. Areas where the density of the material is less than 10% of the initial density before the irradiation are not shown in the plots.

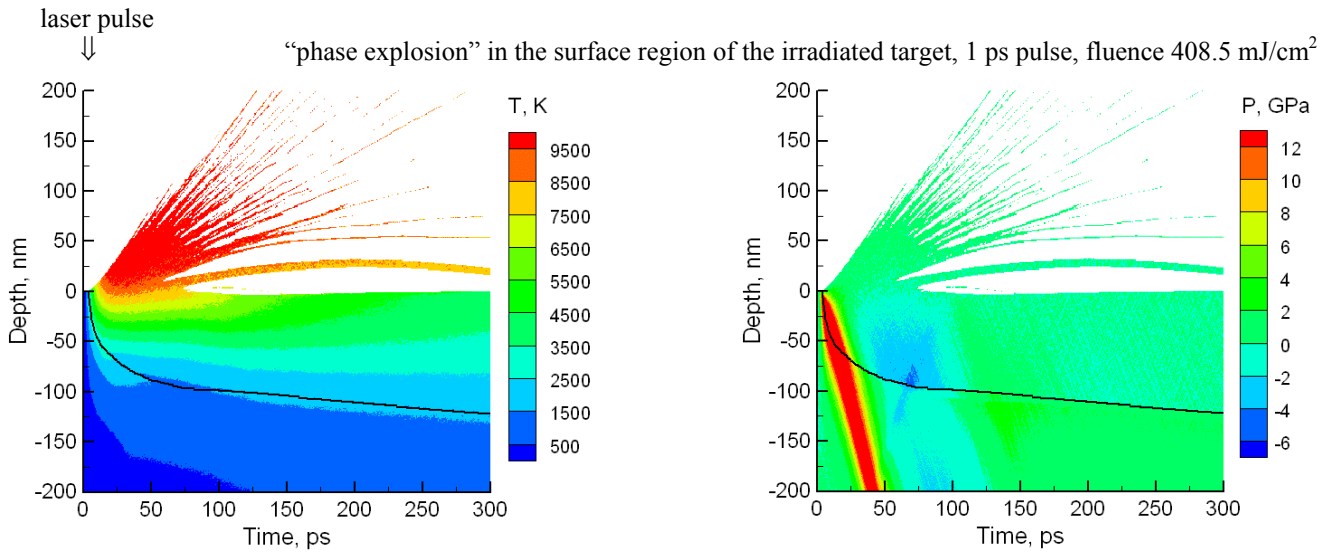

Figure 6. Temperature (a) and pressure (b) contour plots in a simulation of laser ablation driven by an explosive release of vapor in a surface region of a bulk Ni target irradiated with a 1 ps laser pulse at an absorbed fluence of 408.5 mJ/cm^2. Laser pulse is directed along the Y-axes, from the top of the contour plots. Black line separates the melted region from the crystalline bulk of the target. Areas where the density of the material is less than 10% of the initial density before the irradiation are not shown in the plots.

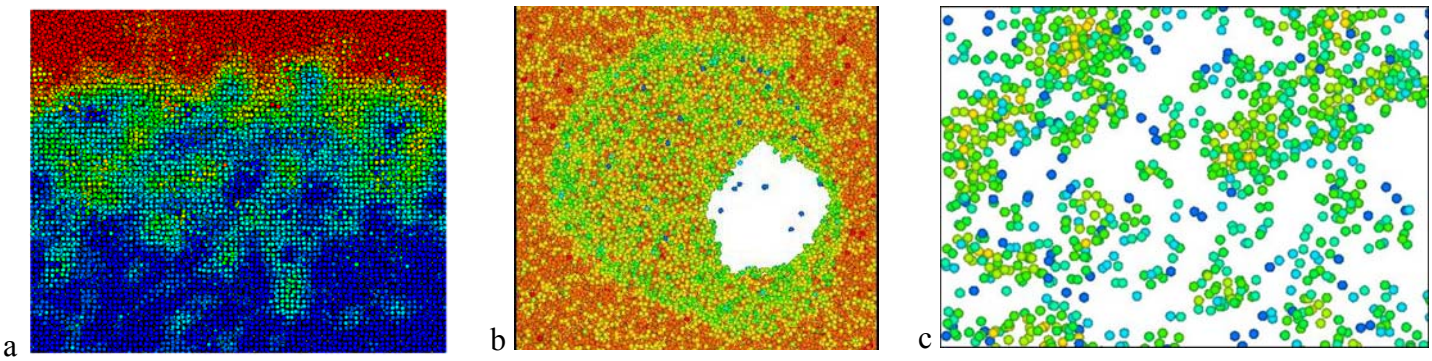

Figure 7. Atomic-level pictures illustrating the melting (a), spallation (b) and phase explosion (c) processes observed in simulations of 1 ps laser irradiation of a bulk Ni target. The images are from simulations performed at absorbed fluences of 193.5 mJ/cm^2 (a, b) and 408.5 mJ/cm^2. In (a) atoms are colored according to the local order parameter (blue atoms have local crystalline surroundings; red atoms belong to the liquid phase), in (b, c) atoms are colored by their potential energy. Only thin slices of the computational cell are shown in (b, c).

A characteristic signature of the transition to this ablation regime is an explosive release of the large amount of vapor that provides the driving force for the decomposition and collective ejection (ablation) of the overheated layer of the target. The drastic increase of the number of ejected monomers is observed at the threshold for the "thermal" ablation in Figure 8. Interestingly, the transition to the ablation regime does not correspond to the increase in the total amount of the material removed from the target.

The picture of the homogeneous expansion of the overheated material and spontaneous decomposition into individual molecules and liquid droplets observed in the simulation is consistent with the "phase explosion" mechanism predicted from classical thermodynamics, e.g. [23-26] and confirmed in earlier simulations of laser ablation [2,3,21,27]. It has been discussed that short pulse laser irradiation can overheat a part of the absorbing region beyond the limit of thermodynamic stability of the target material, leading to the onset of intense temperature, pressure, and density fluctuations. The fluctuations in the thermodynamically unstable material do not disappear but grow, leading to a rapid phase transition of the overheated material into a mixture of gas phase molecules and liquid droplets. The relative amount of the gas phase molecules is related to the degree of overheating and provides a driving force for the expansion of the ablation plume.

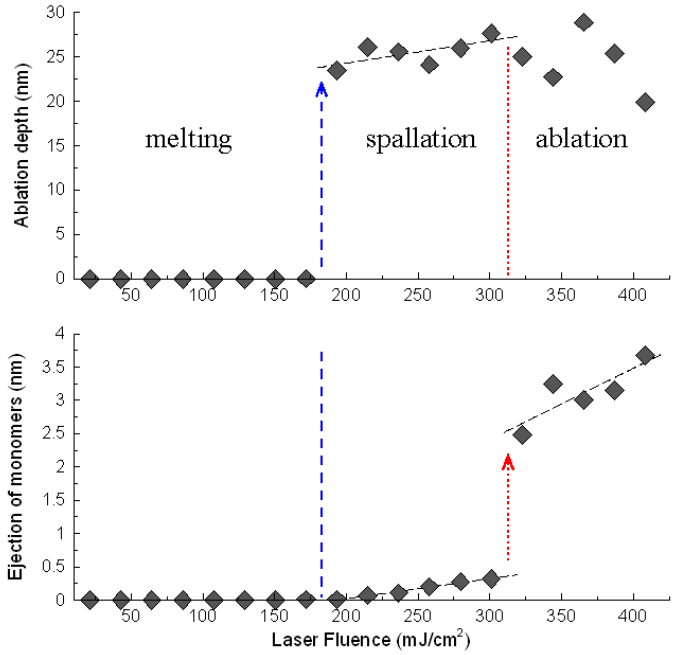

Figure 8. Total ablation yield (a) and the number of gas-phase molecules (b) ejected as a function of laser fluence in simulations of 1 ps laser interaction with bulk Ni targets.

4. SUMMARY

The mechanisms of short pulse laser interaction with metal targets are systematically investigated in a series of simulations performed with a hybrid atomistic-continuum model. The material response to laser irradiation is investigated in three regimes corresponding to the melting and resolidification of the surface region of the target, photomechanical spallation of a single or multiple layers/droplets, and ablation driven by the thermodynamic driving forces. The conditions leading to the transitions between the different regimes and the atomic level characteristics of the involved processes are established.

In the melting regime, the fast homogeneous melting followed by resolidification at fluences close to the melting threshold is turning into two-stage melting with fast homogeneous and slower heterogeneous stages at higher fluences. The slow heterogeneous melting is taking hundreds of picoseconds and is fueled by the energy flowing through the liquid-crystal interface from the hot surface region to the bulk of the target. The onset of spallation interrupts the heat conduction from the hot spalled layer to the bulk of the target and reduces the melting zone.

The onset of spallation corresponds to the condition when the tensile stresses generated in the process of the relaxation of the laser induced compressive pressure exceed the dynamic strength of the material. The region of spallation is shifted toward the irradiated surface with respect to the depth where the maximum tensile stresses are created – the voids appear and evolve in a wide sub-surface region defined by the balance between the tensile stresses and thermal softening of the material. Spallation is always preceded by melting, no spallation of a solid target is observed in the simulations. Spallation of multiple liquid layers/droplets is observed at higher laser fluences.

Transition to the ”phase explosion” regime is signified by a an explosive release of the large amount of vapor that provides the driving force for the decomposition and collective ejection (ablation) of the overheated layer of the target. The total amount of material removed by the laser pulse, however, does not increase at the onset of the phase explosion.

ACKNOWLEDGMENTS

Financial support of this work is provided by the NSF through Award No. CTS-0348503.

REFERENCES

[1] R. F. W. Herrmann, J. Gerlach, E. E. B. Campbell, Ultrashort pulse laser ablation of silicon: an MD simulation study, *Appl. Phys. A* 66, 35-42 (1998).

[2] L. V. Zhigilei, E. Leveugle, B. J. Garrison, Y. G. Yingling, and M. I. Zeifman, Computer simulations of laser ablation of molecular substrates, *Chem. Rev.* **103**, 321-348 (2003).

[3] C. R. Cheng and X. F. Xu, Mechanisms of decomposition of metal during femtosecond laser ablation, *Phys. Rev. B* **72**, 165415 (2005).

[4] X. W. Wang, Large-scale molecular dynamics simulation of surface nanostructuring with a laser-assisted scanning tunnelling microscope, *J. Phys. D: Appl. Phys.* **38**, 1805-1823 (2005).

[5] T. Okamoto, E. Ohmura, T. Sano, Y. Morishige, and I. Miyamoto, Analytical study on metal microstructures using femtosecond laser, *Appl. Phys. A* **81**, 639-643 (2005).

[6] A. K. Upadhyay and H. M. Urbassek, Melting and fragmentation of ultra-thin metal films due to ultrafast laser irradiation: a molecular-dynamics study, *J. Phys. D: Appl. Phys.* **38**, 2933-2941 (2005).

[7] P. Lorazo, L. J. Lewis, and M. Meunier, Thermodynamic pathways to melting, ablation, and solidification in absorbing solids under pulsed laser irradiation, *Phys. Rev. B* **73**, 134108 (2006).

[8] D. S. Ivanov and L. V. Zhigilei, Combined atomistic-continuum modeling of short pulse laser melting and disintegration of metal films, *Phys. Rev. B*, **68**, 064114 (2003).

[9] D. S. Ivanov and L. V. Zhigilei, The effect of pressure relaxation on the mechanisms of short pulse laser melting, *Phys. Rev. Lett.* **91**, 105701 (2003).

[10] D. S. Ivanov and L. V. Zhigilei, Combined atomistic - continuum model for simulation of laser interaction with

metals: application to calculation of melting thresholds in Ni targets of varying thickness, *Appl. Phys. A* **79**, 977-981 (2004).

[11] Z. Lin and L. V. Zhigilei, Time-resolved diffraction profiles and atomic dynamics in short pulse laser induced structural transformations: Molecular dynamics study, *Phys. Rev. B* **73**, 184113 (2006).

[12] C. Schäfer, H. M. Urbassek, and L. V. Zhigilei, Metal ablation by picosecond laser pulses: A hybrid simulation, *Phys. Rev. B* **66**, 115404 (2002).

[13] E. Leveugle, D. S. Ivanov, and L. V. Zhigilei, Photomechanical spallation of molecular and metal targets: molecular dynamics study, *Appl. Phys. A* **79**, 1643-1655 (2004).

[14] D. S. Ivanov, L. V. Zhigilei, E. M. Bringa, M. De Koning, B. A. Remington, M. J. Caturla, and S. M. Pollaine, Molecular dynamics simulations of shocks including electronic heat conduction and electron-phonon coupling, *Shock Compression of Condensed Matter - 2003*, *AIP Conference Proceedings* **706**, 225-228 (2004).

[15] L. V. Zhigilei and D. S. Ivanov, Channels of energy redistribution in short-pulse laser interactions with metal targets, *Appl. Surf. Sci.* **248**, 433-439 (2005).

[16] L. V. Zhigilei and B. J. Garrison: Mat. Res. Soc. Symp. Proc. **538**, 491 (1999). L. V. Zhigilei and B. J. Garrison, Pressure waves in microscopic simulations of laser ablation, Mat. Res. Soc. Symp. Proc. **538**, 491-496 (1999).

[17] X. W. Zhou, H. N. G. Wadley, R. A. Johnson, D. J. Larson, N. Tabat, A. Cerezo, A. K. Petford-Long, G. D. W. Smith, P. H. Clifton, R. L. Martens, and T. F. Kelly, Atomic scale structure of sputtered metal multilayers, Acta Mater. **49**, 4005-4015 (2001).

[18] L. V. Zhigilei, D. S. Ivanov, E. Leveugle, B. Sadigh, and E. M. Bringa, Computer modeling of laser melting and spallation of metal targets, *High-Power Laser Ablation V*, edited by C. R. Phipps, *Proc. SPIE* **5448**, 505-519 (2004).

[19] P. Chen, I. V. Tomov, and P. M. Rentzepis, Laser-induced transient structure and stress in a platinum (111)crystal studied by time-resolved X-ray diffraction, *J. Appl. Cryst.* **32**, 82-88, (1999).

[20] K. Sokolowski-Tinten, J. Bialkowski, M. Boing, A. Cavalleri, and D. von der Linde, Thermal and nonthermal melting of gallium arsenide after femtosecond laser excitation, *Phys. Rev. B* **58**, R11805-R11808 (1998).

[21] L. V. Zhigilei and B. J. Garrison, Microscopic mechanisms of laser ablation of organic solids in the thermal and stress confinement irradiation regimes, *J. Appl. Phys.* **88**, 1281-1298 (2000).

[22] A. G. Zhidkov, L. V. Zhigilei, A. Sasaki, and T. Tajima, Short-laser-pulse driven emission of energetic ions into a solid target from a surface layer spalled by a laser prepulse, *Appl. Phys. A* **73**, 741-747 (2001).

[23] M. M. Martynyuk, Mechanism for metal damage by intense electromagnetic radiation, *Sov. Phys. Tech. Phys.* **21**, 430-433 (1976).

[24] J. Sunner, M. G. Ikonomou, P. Kebarle, SIMS spectra of alcohols and the phase explosion model of desorption ionization, *Int. J. Mass Spectrom.* **82**, 221-237 (1988).

[25] A. Miotello and R. Kelly, Laser-induced phase explosion: new physical problems when a condensed phase approaches the thermodynamic critical temperature, *Appl. Phys. A* **69**, S67-S73 **(**1999)

[26] N. M. Bulgakova and I. M. Bourakov, Phase explosion under ultrashort pulsed laser ablation: modeling with analysis of metastable state of melt, *Appl. Surf. Sci*. **197**, 41-44 (2002).

[27] L. V. Zhigilei, Dynamics of the plume formation and parameters of the ejected clusters in short-pulse laser ablation, *Appl. Phys. A* **76**, 339-350 (2003).